The Astrophysical Journal Letters, 863:L33 (7pp), 2018 August 20 https://doi.org/10.3847/2041-8213/aad868

Discovery of Extended Main Sequence Turnoffs in Galactic Open Clusters

A. F. Marino[1], A. P. Milone[2], L. Casagrande[1], N. Przybilla[3], L. Balaguer-Núñez[4,5], M. Di Criscienzo[6], A. Serenelli[5,7], and F. Vilardell[5]
[1] Research School of Astronomy & Astrophysics, Australian National University, Canberra, ACT 2611, Australia; anna.marino@anu.edu.au
[2] Dipartimento di Fisica e Astronomia "Galileo Galilei," Univ. di Padova, Vicolo dell'Osservatorio 3, Padova, I-35122, Italy
[3] Institut für Astro- und Teilchenphysik, Universität Innsbruck, Technikerstrasse 25, A-6020, Innsbruck, Austria
[4] Departament de Fisica Quantica i Astrofisica (Facultat de Fisica), Universitat de Barcelona, Marti i Franques 1, E-08028, Barcelona, Spain
[5] Institut d'Estudis Espacials de Catalunya (IEEC), C/Gran Capita, 2-4, E-08034, Barcelona, Spain
[6] INAF—Osservatorio Astronomico di Roma, Monte Porzio, Italy
[7] Institute of Space Sciences (ICE, CSIC) Campus UAB, Carrer de Can Magrans, s/n, E-08193, Barcelona, Spain
Received 2018 July 16; revised 2018 August 4; accepted 2018 August 6; published 2018 August 17

Abstract

The color–magnitude diagrams (CMDs) of Galactic open clusters are widely considered to be the prototypes of single stellar populations. By using photometry in ultraviolet and optical bands we discovered that the nearby young cluster NGC 6705 (M11) exhibits an extended main-sequence turnoff (eMSTO) and a broadened main sequence (MS). This is the first evidence of multiple stellar populations in a Galactic open cluster. By using high-resolution Very Large Telescope (VLT) spectra we provide direct evidence that the multiple sequences along the CMD correspond to stellar populations with different rotation rates. Specifically, the blue MS (bMS) is formed of slow-rotating stars, while red-MS (rMS) stars are fast rotators. Moreover, we exploit photometry from *Gaia* data release 2 (DR2) to show that three Galactic open clusters, namely NGC 2099, NGC 2360, and NGC 2818, exhibit the eMSTO, thus suggesting that it is a common feature among these objects. Our previous work on the Large Magellanic Cloud star cluster NGC 1818 shows that slowly and rapidly rotating stars populate the bMS and rMS observed in its CMD. The similarities between M11 and the young clusters of the Magellanic Clouds (MCs) suggest that rotation is responsible for the appearance of multiple populations in the CMDs of both Milky Way open clusters and MCs young clusters.

Key words: Hertzsprung–Russell and C–M diagrams – open clusters and associations: individual (NGC 6705, NGC 2099, NGC 2360, NGC 2818)

1. Introduction

The Galactic open clusters are considered to be the prototypes of simple stellar populations. This assumption was supported by color–magnitude diagrams (CMDs) often well reproduced by single isochrones (e.g., Kalirai et al. 2003; Bedin et al. 2010). In contrast, the CMDs of young and intermediate-age star clusters in both Magellanic Clouds (MCs) are not consistent with single isochrones. Nearly all of these clusters with ages between ∼700 Myr and ∼2 Gyr exhibit extended main sequence turnoff (eMSTO; e.g., Mackey & Broby Nielsen 2007; Milone et al. 2009; Goudfrooij et al. 2011, 2014); and clusters younger than ∼700 Myr show both split main sequence (MS) and eMSTO (e.g., Milone et al. 2013, 2015, 2018; Correnti et al. 2015, 2017; Bastian et al. 2017; Li et al. 2017).

Stellar rotation plays a major role in the split MS and the eMSTO. The comparison between the observed CMDs of young MCs clusters and isochrones indicates that the blue MS (bMS) is consistent with a population of non-rotating or slow-rotating stars, while red-MS (rMS) stars rotate close to the critical value. According to this scenario, the fainter part of the main sequence turnoff (MSTO) is mainly populated by fast rotators, while the upper MSTO should host slow rotators (e.g., D'Antona et al. 2015). This scenario is confirmed by the large fraction of Be stars in young MCs clusters (e.g., Keller et al. 2000; Bastian et al. 2017), mostly populating the rMS and the faint MSTO (Milone et al. 2018). Spectroscopic analysis of the Large Magellanic Cloud (LMC) cluster NGC 1866 has provided direct evidence that its eMSTO hosts stars with different rotations, and that the faint MSTO is mostly populated by fast rotators (Dupree et al. 2017). High-resolution spectra have shown that the split MS of the LMC cluster NGC 1818 hosts a bMS made of slow rotators, and a rMS of stars with high rotation (Marino et al. 2018).

Stellar rotation is a common phenomenon that affects many aspects of stellar evolution, in particular for stars with $\mathcal{M} >$ 1.5–1.7 $\mathcal{M}_{\odot}$ (Meynet & Maeder 2000, and references therein). Stars with rotation rates from slow to nearly critical have been indeed reported both in field and open cluster stars (e.g., Huang et al. 2010), and the possible role of stellar rotation in causing color spreads in some open clusters was suggested by Brandt & Huang (2015a, 2015b).

We combine Strömgren photometry and spectra of the Galactic open cluster NGC 6705 (M11) to investigate its MSTO and upper MS. As estimated by Cantat-Gaudin et al. (2014), the age of this cluster ranges from 250 to 320 Myr, and its mass is between 3700 and 11,000 $\mathcal{M}_{\odot}$. We further exploit photometry, proper motions, and parallaxes from *Gaia* data release 2 (DR2; Gaia Collaboration et al. 2018) to search for multiple populations in Galactic open clusters NGC 2099, NGC 2360, and NGC 2818.

2. Data and Analysis

To search for multiple sequences along the CMD of M11 we used images collected with the Isaac Newton Telescope (INT) through the *uvy* filters as part of the Strömgren survey for asteroseismology and Galactic archeology (Casagrande et al. 2014).

Specifically, we used 10 s + 2 × 20 s + 2 × 50 s + 2 × 120 s u band, 5 s + 2 × 10 s + 2 × 40 s + 2 × 120 s v band, and 3 × 3 s + 2 × 5 s + 2 × 50 s y band images; stellar parallaxes and proper motions are from *Gaia* DR2.

The photometry and astrometry of the INT images was carried out using kitchensync (Anderson et al. 2008) modified for INT images. For each exposure we derived a grid of 3 × 3 empirical point spread functions (PSFs) by using the available isolated, bright, and non-saturated stars. We accounted for the spatial variation of the PSF by assuming that each star of each image is associated to a bi-linear weighted interpolation of the four nearest PSFs (Anderson & King 2000).

The fluxes of bright and faint stars have been derived by using distinct procedures. Bright stars have been measured in each exposure independently by using the best PSF model, and then averaged together. To derive fluxes and positions of faint stars, poorly constrained in the single exposures, we fitted all pixels of all exposures simultaneously (see Anderson et al. 2008). The photometry has been calibrated as in Casagrande et al. (2014, see their Section 2).

Cluster members have been selected by using proper motions and parallaxes from *Gaia* DR2 (see Section 3). The photometry of the cluster members has been corrected for differential reddening as in Milone et al. (2012).

The spectroscopic data consist of Fibre Large Array Multi Element Spectrograph (FLAMES)/GIRAFFE data (Pasquini et al. 2002), with setup H665 ($R \sim \lambda/\Delta\lambda \sim 17{,}000$), collected under the *Gaia*-European Southern Observatory (ESO) Survey (Gilmore et al. 2012) and publicly available on the ESO archive.[8] From the available sample of stars observed in M11, we have selected those in the magnitude range $12.0 \lesssim v \lesssim 14.5$, which is the interval where the spread MS and MSTO is observed (see Section 3). At the Hα line wavelength, the typical signal-to-noise of the fully reduced spectra is ∼100.

Projected rotational velocities ($v \sin i$) were determined by fitting the Hα core. A grid of hybrid non-local thermodynamic equilibrium (non-LTE) model spectra was computed using the approach discussed by Przybilla & Butler (2004a, 2004b) based on ATLAS9 model atmospheres (Kurucz 1993). Non-LTE level populations were calculated using DETAIL and synthetic spectra using SURFACE (Giddings 1981; Butler & Giddings 1985, both updated by K. Butler). The grid covers effective temperatures $T_{\rm eff}$ from 6400 to 8800 K (step width of 200 K), with surface gravity fixed to $\log g = 4.0$, which is the typical value found in the *Gaia*-ESO survey for these stars. The consideration of non-LTE effects, yielding a pronounced strengthening of the Hα Doppler core, is important for avoiding a systematic bias of the $v \sin i$ in particular for slower rotators. The model spectra were convolved with a Gaussian profile to account for instrumental broadening and a rotational profile $v \sin i$ from 0 to 300 km s^{-1} (step width of 20 km s^{-1}).

We employed a χ^2 minimization of each observed spectrum around the Hα line to simultaneously infer $T_{\rm eff}$, primarily affecting the wings, and $v \sin i$, which has a major impact on the core. The inferred $v \sin i$ values are listed in Table 1.

The choice of atmospheric parameters has little impact on the $v \sin i$ determination. Varying $\log g$ by ±0.5 dex has negligible effect, while changes in $T_{\rm eff}$ by ±200 K result in $v \sin i$ variations of ∓20 km s^{-1}. The major contribution to the errors is associated with the continuum placement, which introduces an internal uncertainty of ±30–40 km s^{-1}. Conservatively, we associate an internal error of ±40 km s^{-1} to our $v \sin i$ estimates.

[8] http://archive.eso.org/cms.html

Table 1
Identifiers from the *Gaia*-ESO Survey, Projected Rotational Velocities ($v \sin i$), and Photometry (v–($u - v$)) for Our Spectroscopic Targets

ID (*Gaia*-ESO)	$v \sin i$ (km s^{-1})	v	$u - v$ (mag)	CMD Region
18510414-0616202	270	12.57	1.34	eMSTO
18510358-0616573	178	12.77	1.40	eMSTO
18511514-0614431	212	12.74	1.50	eMSTO
18505981-0615291	138	12.09	1.50	eMSTO
18505829-0615284	139	12.60	1.43	eMSTO
18510593-0614348	130	11.82	1.52	eMSTO
18505407-0616503	76	12.10	1.42	eMSTO
18510656-0614562	47	12.08	1.30	eMSTO
18510793-0617217	99	12.32	1.39	eMSTO
18505098-0615314	176	12.87	1.54	eMSTO
18505254-0617374	180	12.49	1.53	eMSTO
18510577-0615230	220	12.68	1.39	eMSTO
18505436-0614545	202	12.78	1.40	eMSTO
18510462-0616124	17	12.94	1.32	eMSTO
18511517-0615541	117	12.25	1.76	eMSTO
18510512-0614075	30	13.87	1.32	bMS
18510368-0617353	42	13.41	1.24	bMS
18510392-0613560	58	13.94	1.34	bMS
18510407-0618579	114	14.00	1.33	bMS
18505693-0616214	80	13.34	1.30	bMS
18505473-0615364	98	13.63	1.26	bMS
18510907-0618579	105	13.32	1.29	bMS
18510214-0616502	154	13.39	1.29	bMS
18511287-0617194	150	14.13	1.33	bMS
18505682-0617071	18	13.96	1.33	bMS
18511086-0616295	39	13.57	1.28	bMS
18511441-0614423	103	13.57	1.29	bMS
18510255-0614488	240	13.30	1.39	rMS
18505208-0617321	261	13.97	1.41	rMS
18511127-0615520	182	14.04	1.45	rMS
18510452-0615406	268	13.68	1.42	rMS
18510092-0618029	172	13.95	1.37	rMS
18510099-0616523	184	13.07	1.38	rMS
18505944-0618212	210	13.67	1.39	rMS
18510522-0615219	145	13.96	1.42	rMS
18510572-0617177	199	13.21	1.39	rMS
18510687-0617537	190	13.59	1.37	rMS
18505345-0616096	215	13.75	1.37	rMS
18510143-0617510	270	13.74	1.45	rMS
18510176-0614073	100	13.04	1.36	rMS
18510737-0618226	279	13.79	1.41	rMS
18511195-0618463	278	13.50	1.38	rMS
18505296-0617402	87	14.02	1.43	rMS
18510286-0615250	86	14.17	1.46	rMS
18505244-0618002	227	13.20	1.42	rMS
18510891-0616433	210	13.22	1.38	rMS
18505573-0617293	220	13.84	1.40	rMS
18511094-0615043	35	13.84	1.43	rMS
18511164-0618114	260	14.26	1.45	rMS
18511196-0619220	141	13.33	1.36	rMS
18510126-0615287	⋯	12.44	1.41	Hα emission
18510488-0614370	⋯	12.89	1.44	Hα emission
18505844-0613451	⋯	12.53	1.34	Hα emission
18511063-0618531	⋯	12.56	1.55	Hα emission
18505950-0615397	⋯	13.56	1.44	Hα emission
18505883-0616295	⋯	13.22	1.38	Hα emission
18505797-0615472	⋯	13.13	1.37	Hα emission

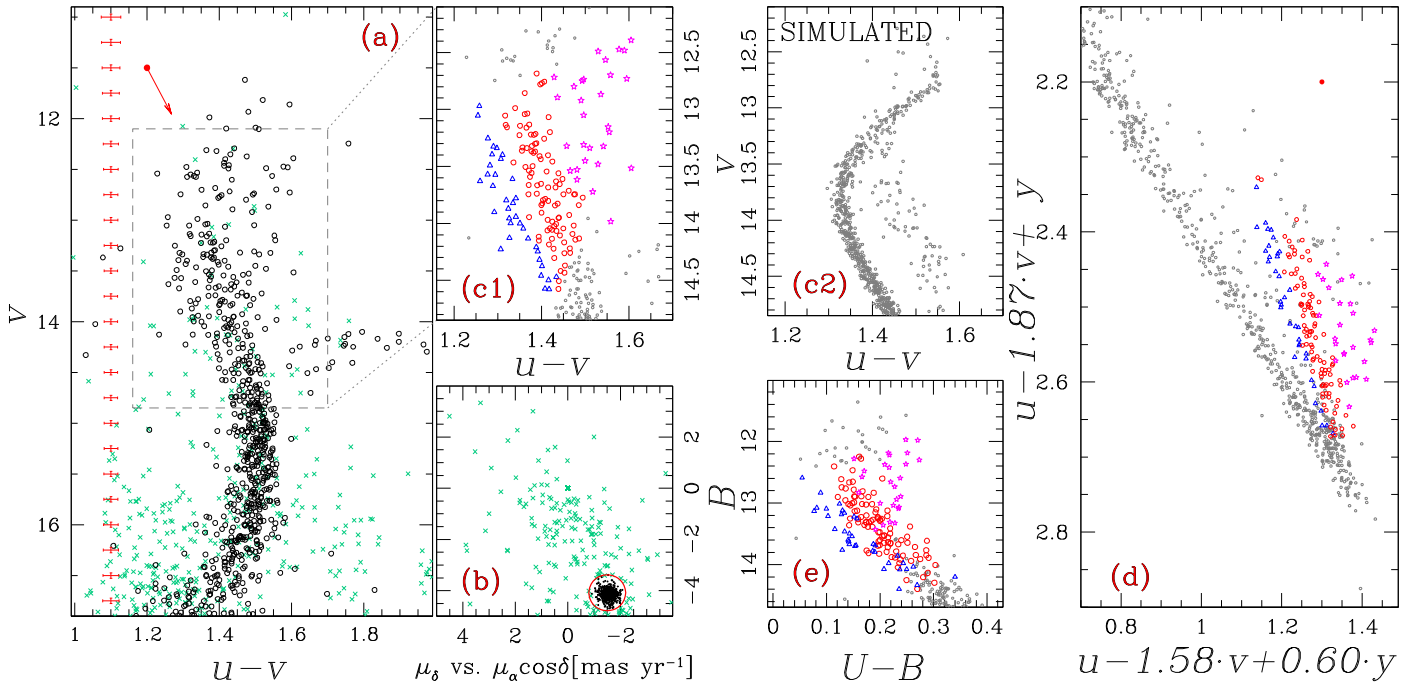

Figure 1. Panel a: v–$(u-v)$ CMD corrected for differential reddening of stars in the M11 field. Cluster members and field stars are plotted with black circles and aqua crosses, respectively. The red arrow indicates the reddening vector. Typical photometric uncertainties are plotted on the left. Panel b: vector-point diagram of proper motions for the stars in the CMD. The red circle separates the bulk of cluster members from field stars. Panel c1: zoom-in of the CMD around the MSTO. bMS, rMS, and eMSTO stars are represented with blue triangles, red circles, and magenta star-like symbols, respectively. The same colors and symbols are used in the other panels. Panel c2: synthetic sv–$(u-v)$ CMD for one non-rotating population from a Geneva isochrone (Georgy et al. 2013) with age = 250 Myr, $Z = 0.014$, $(m-M)_0 = 10.85$, $E(B-V) = 0.40$. Panel d: reddening-free diagram for cluster members. Panels e: differential reddening corrected B–$(U-B)$ CMD (photometry by Sung et al. 1999).

3. The Extended Main-sequence Turnoff of M11

The v–$(u-v)$ CMD of stars in the M11 field is plotted in Figure 1(a). The vector-point diagram of proper motions plotted in Figure 1(b) reveals that M11 stars are clearly clustered around $(\mu_\alpha \cos\delta;\ \mu_\delta) = (\sim -1.57;\ -4.12)$ mas yr^{-1}, while the proper motions of field stars exhibit a broadened distribution. As a further membership criterium, we estimated the median parallax of the proper-motion selected stars ($\langle\omega\rangle = 0.42$ mas) and considered as members of M11 only stars with parallaxes within 0.17 mas (corresponding to three times the dispersion) from the median value. We verified that the selected sample of cluster members matches the M11 stars selected by Cantat-Gaudin et al. (2018).

The CMD of cluster members reveals that M11 hosts an eMSTO and a broadened, possibly split, upper MS, in close analogy with MC clusters at similar ages. The color and magnitude broadening of the eMSTO and of the upper MS are significantly larger than those expected by observational errors. The presence of these features is confirmed by the synthetic v versus $(u-v)$ CMD (Figure 1(c2)) corresponding to one single non-rotating population, which does not show any evidence of either eMSTO or spread MS. The MS region with $v > 14.5$ is consistent with a single stellar sequence.

To further demonstrate that the eMSTO and the broadened MS are not artifacts due to residual differential reddening, we selected three groups of bMS stars, rMS stars, and eMSTO stars by hand in the v versus $u-v$ CMD plotted in Figure 1 (c1). In Figure 1(d) we plotted the magnitude combination $u - 1.87 \cdot v + y$ against $u - 1.58 \cdot v + 0.60 \cdot y$ for cluster members. This diagram is reddening-free by assuming for the M11 field of view the absorption coefficients by Schlegel et al. (1998). If the eMSTO and broadened MS are due to residual differential reddening, we would expect that the three stellar groups exhibit random values of the reddening-free quantities $u - 1.87 \cdot v + y$ and $u - 1.58 \cdot v + 0.60 \cdot y$. The fact that the three groups of bMS, rMS, and eMSTO stars are clearly separated in the reddening-free diagram demonstrates that eMSTO and broadened MS are intrinsic features of M11. Panel e shows the B versus $(U-B)$ CMD from Sung et al. (1999) corrected for differential reddening. The selected bMS, rMS, and eMSTO stars populate distinct regions of this diagram, thus corroborating the presence of multiple stellar populations in M11.

4. Rotation

The position of our spectroscopically analyzed stars on the v–$(u-v)$ CMD is shown in the left-upper panel of Figure 2. They are distributed along the eMSTO and the broadened MS of M11, discussed in Section 3. The sidebar shows the color scale indicative of the inferred $v \sin i$. Stars exhibiting an Hα emission core have been clearly indicated. Our projected rotational velocities results suggest that $v \sin i$ values span a large range, from a few tens to more than 250 km s^{-1}, and that stars with slower rotation are distributed on the bluer side of the CMD.

For comparison reasons, the synthetic CMD of Figure 1(c2) for a non-rotating stellar population has been reproduced in the left-bottom panel of Figure 2. To this non-rotating population we have added a synthetic coeval rapidly rotating population, with $\omega = 0.9\omega_{\rm crit}$ (Georgy et al. 2013). If a rotation regime close to the critical velocity can account for a spread in the MSTO, the split MS can only be reproduced by two stellar populations with intrinsic different stellar rotation rates.

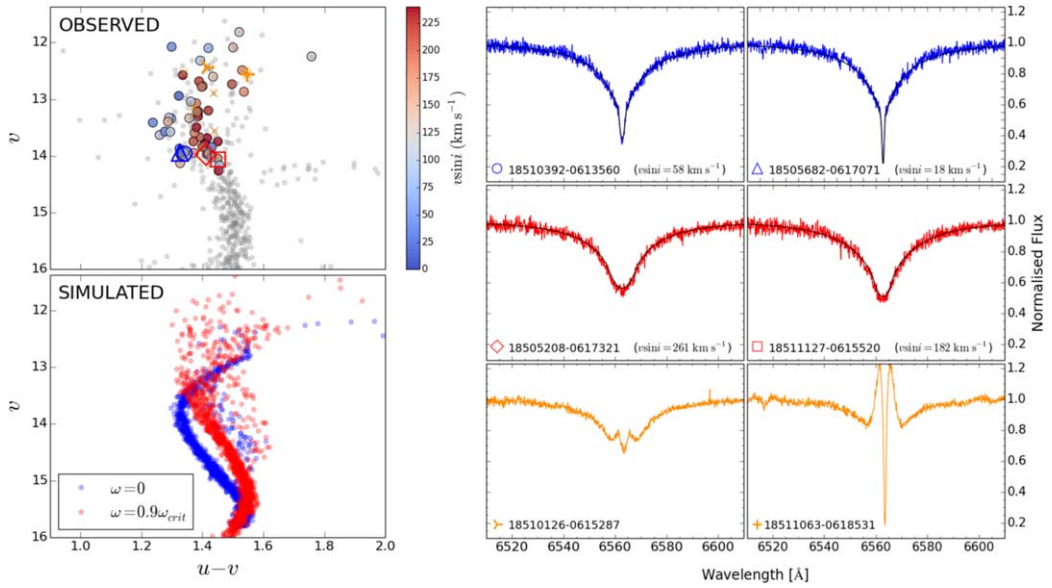

Figure 2. Left-upper panel: observed v–$(u-v)$ CMD of M11. Spectroscopically analyzed stars are marked with large circles. The color of each circle is associated with the corresponding value of $v \sin i$ as indicated by the color scale on the right. Left-lower panel: v–$(u-v)$ synthetic CMD corresponding to two coeval populations (age = 250 Myr), one with no rotation (blue) and the other with high rotation ($\omega = 0.9\omega_{\rm crit}$, red). The expected photometric error has been added to the simulations Right panels: some examples of our spectra. From the upper to lower panels we show two bMS and two rMS at similar magnitude, and two Hα core emission stars. For each bMS and rMS spectrum, we superimpose to the observed spectra the best-fitting non-LTE model in black.

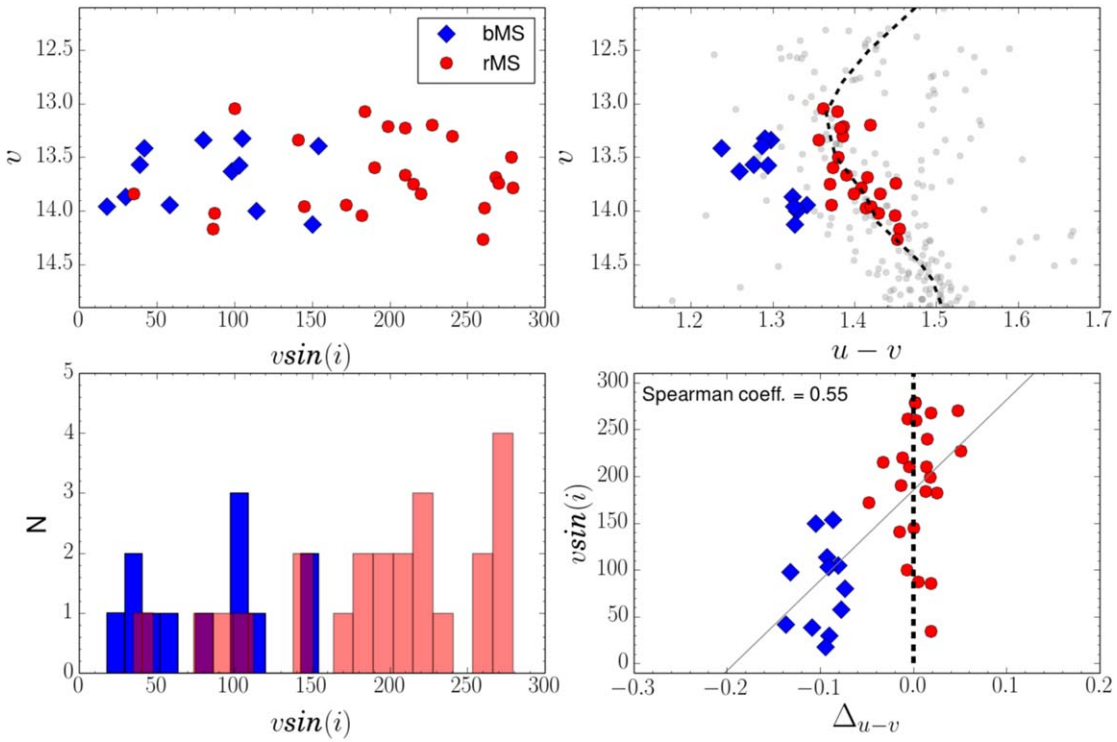

Figure 3. Left: v mag vs. $v \sin i$ for MS stars in M11 (upper panel); on the lower panel we show the histogram distribution of $v \sin i$ for rMS (red) and bMS (blue). Right: v–$(u-v)$ CMD zoomed on the MS. The black-dashed line is a fiducial for the rMS (upper panel). The lower panel shows $v \sin i$ as a function of the difference between the $(u-v)$ color of each MS star and the color of the fiducial (Δ_{u-v}). The black-dashed line corresponds to $\Delta_{u-v} = 0$. In all panels rMS and bMS are represented with red-filled circles and blue diamonds, respectively.

The right panels of Figure 2 illustrate some examples of our spectral fitting. Specifically, the upper and middle panels show two bMS and rMS stars, respectively, chosen to have similar luminosities. The best-fit synthetic spectra are superimposed to each spectrum. The lower panels display the spectra of two Hα-emission stars in our sample, for which we could not infer any $v \sin i$. A visual inspection of these spectra immediately suggests a different $v \sin i$ for the bMS and rMS stars, having a similar luminosity but a different color. The spectral profiles of the two rMS stars are significantly broader than those of the bMS ones.

Figure 3 is a closer look at MS. The location on the CMD of the MS stars with available spectroscopy is displayed for stars

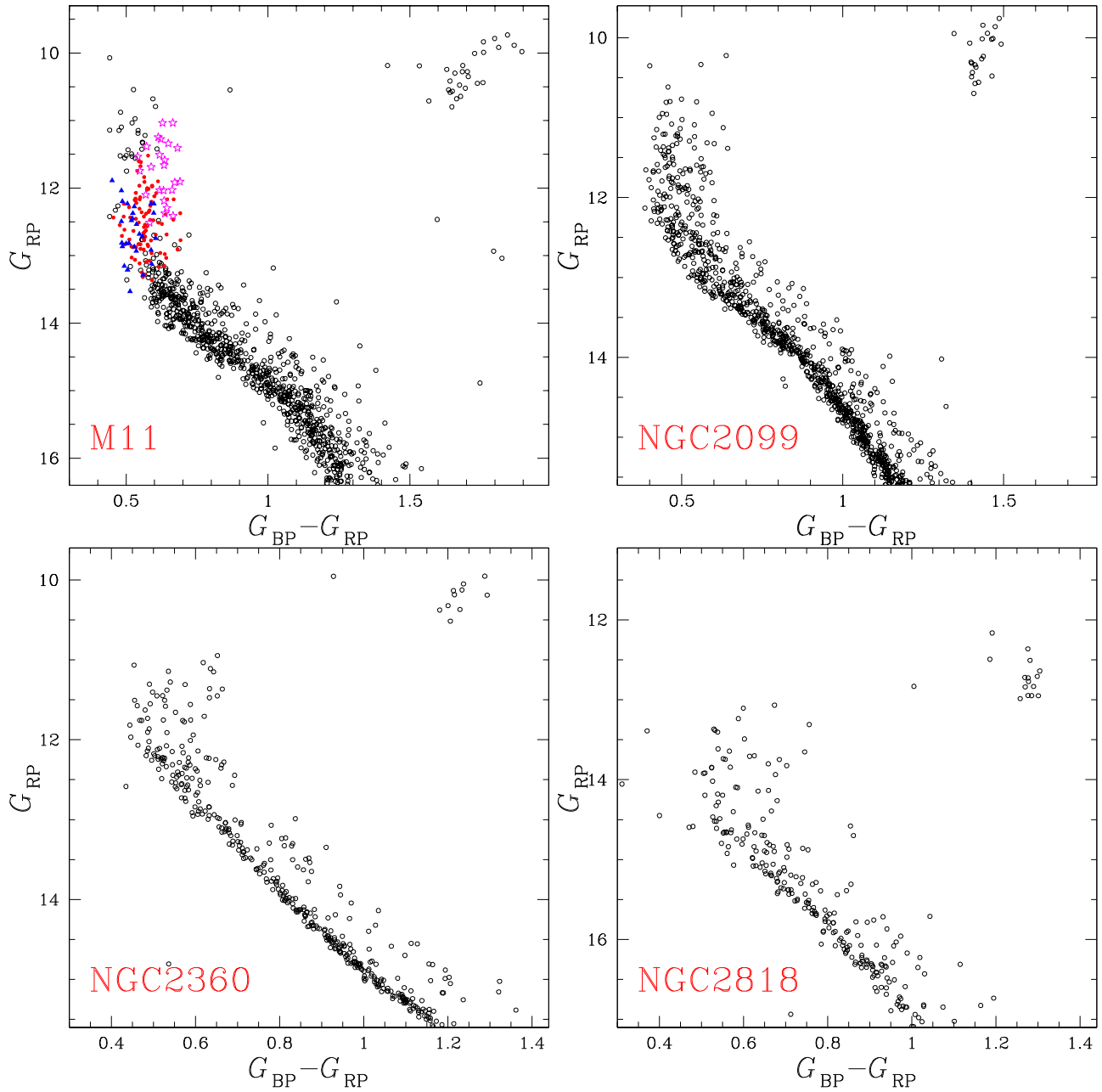

Figure 4. CMDs from *Gaia* DR2 photometry of Galactic open clusters M11, NGC 2099, NGC 2360, and NGC 2818, exhibiting an eMSTO. The three groups of bMS, rMS, and eMSTO stars of M11, selected in Figure 1, are colored blue, red, and magenta, respectively. The binaries sequence is clearly distinguishable in the CMDs of NGC 2099, NGC 2360, and NGC 2818.

with $v \gtrsim 13$. Our targets are clearly distributed on the split MS of M11, and the association with the bMS and rMS is straightforward (right-upper panel).

The $v \sin i$ histogram distributions, shown in the lower-left panel, illustrate the quite wide range for both the bMS and rMS. bMS stars do not show any value $\gtrsim$150 km s^{-1}. As $v \sin i$ values are lower limits to the real stellar rotation, depending on the inclination, more likely, a fast-rotating star has a higher $v \sin i$ than a slow rotator. Although a certain degree of overlap in $v \sin i$ between bMS and rMS might be expected because of projection effects, we cannot exclude some slower rotators among the rMS.

The left-upper panel of Figure 3 displays the v magnitude versus $v \sin i$ for rMS and bMS stars. Clearly, bMS stars are slower rotators, while the rMS hosts stars with higher rotation. In the right panels we analyze the color of the MS stars as a function of $v \sin i$. To this aim we have drawn a fiducial line by eye defining the rMS on the v–$(u-v)$ CMD (upper-right panel). The difference in color between each star and the fiducial, Δ_{u-v}, within each of the two MSs, does not show any significant trend with $v \sin i$ (lower-right panel).

The average $v \sin i$ we obtain for the 12 bMS and the 23 rMS are $\langle v \sin i \rangle_{\rm bMS} = 83 \pm 14$ km s^{-1} ($\sigma = 46$ km s^{-1}) and $\langle v \sin i \rangle_{\rm rMS} = 194 \pm 15$ km s^{-1} ($\sigma = 68$ km s^{-1}), respectively, meaning that a difference in the rotation regimes of the two MSs exists. The mean $v \sin i$ difference is $\langle \Delta_{v \sin i_{\rm rMS} - v \sin i_{\rm bMS}} \rangle = 111 \pm 21$ km s^{-1}.

5. Extended Main-sequence Turnoff as a Common Feature of Open Clusters: The Cases of NGC 2099, NGC 2360, and NGC 2818

Ultraviolet and optical filters are efficient tools to identify multiple sequences in the CMDs of young clusters. Although in optical filters the split MS and the eMSTO are less prominent than in the ultraviolet, these features can be detected also in purely optical photometric diagrams (e.g., Milone et al. 2013, 2016; Correnti et al. 2015). As an example, in the upper-left panel of Figure 4, we plot the $G_{\rm RP}$ versus $G_{\rm BP}-G_{\rm RP}$ CMD of M11 cluster members from *Gaia* DR2 photometry. The three groups of bMS, rMS, and eMSTO stars exhibit different colors, further confirming that the CMD of M11 is not consistent with a single isochrone, and demonstrating that *Gaia* photometry is able to detect eMSTOs.

Driven by this result, we started inspecting the *Gaia* DR2 database to search for multiple populations in open clusters. Our first results are shown in Figure 4, where we plot the CMDs for three Galactic open clusters, namely NGC 2099, NGC 2360, and NGC 2818. As for M11, cluster members were selected from *Gaia* DR2 proper motions and parallaxes, and the CMDs were corrected for differential reddening. Noticeably, these clusters exhibit an eMSTO. The MS is much narrower than the eMSTO and its color spread is generally consistent with observational errors, thus demonstrating that the eMSTO is not due to photometric uncertainties or residual differential reddening.

The analysis of a large sample of MCs clusters with ages of ∼40 Myr–2.5 Gyr has demonstrated that eMSTOs are common among these objects, while split MSs are observed in clusters younger than ∼700 Myr (e.g., Milone et al. 2009, 2018), among stars with masses $\gtrsim 1.6\mathcal{M}_{\odot}$. Such mass corresponds to the MS kink associated with the onset of the envelope convection due to the opacity peak of partial H ionization (e.g., D'Antona et al. 2002).

Although an eMSTO is displayed by all of the clusters shown in Figure 4, remarkably a broadened MS is present only in M11 and NGC 2099. By comparing the CMDs of Figure 4 with isochrones from Marigo et al. (2017), we find that these two clusters have ages of ∼300 Myr ∼500 Myr, respectively; NGC 2818 and NGC 2360 are well fitted by ∼800 Myr and ∼1.1 Gyr isochrones. This fact corroborates the conclusion that the eMSTOs and broaden/split MSs observed in the Milky Way clusters originate from the same physical mechanism responsible for the appearance of similar features in the MCs clusters.

6. Conclusions

The eMSTO was first discovered to be a common feature in the CMD of the Large and Small MCs clusters younger than ∼2.5 Gyr (e.g., Mackey & Broby Nielsen 2007; Glatt et al. 2008; Milone et al. 2009, 2018; Goudfrooij et al. 2011, 2014). This finding and the evidence of split MSs in MC clusters younger than ∼800 Myr (e.g., Milone et al. 2015, 2018; Bastian et al. 2017; Correnti et al. 2017) has challenged the theories on the formation and evolution of these objects.

The eMSTO was initially interpreted as the signature of an extended star formation history, with young MC clusters considered to be the counterparts of the old GCs with multiple populations (e.g., Conroy & Spergel 2011; Keller et al. 2011). Alternatively, the eMSTO could be due to coeval stellar populations with different rotation (e.g., Bastian & de Mink 2009).

Recent studies have provided strong evidence that rotation plays a major role in shaping the split MS and the eMSTO. Direct evidence that the rMS is populated by fast rotators, while the bMS hosts stars with low rotation, comes from spectroscopic measurements of MS stars in the LMC cluster NGC 1818 (Marino et al. 2018); evidence for the connection between the eMSTO and stars with different rotation rates has been provided for NGC 1866 (Dupree et al. 2017).

We have combined *uvy* Strömgren photometry and *Gaia* DR2 proper motions and parallaxes to search for multiple populations in the Galactic open cluster M11. The v versus $(u-v)$ CMD shows an eMSTO and a broadened, possibly split, MS in the magnitude interval $12.0 \lesssim v \lesssim 14.5$. We have demonstrated that these are intrinsic features of the M11 CMD, in close analogy with what was previously observed in nearly all of the young clusters of both MCs. This is the first evidence of a connection between the eMSTO in MCs and in Galactic open clusters.

We have exploited GIRAFFE data to derive projected rotational velocities for a sample of stars in M11. Our analysis shows a clear difference in the mean $v \sin i$ between bMS and rMS stars, having average values of $\langle v \sin i\rangle_{\rm bMS} = 83 \pm 14$ km s^{-1} ($\sigma = 46$ km s^{-1}) and $\langle v \sin i\rangle_{\rm rMS} = 194 \pm 15$ km s^{-1} ($\sigma = 68$ km s^{-1}). A large range in $v \sin i$ is also present among eMSTO stars, with some of them showing Hα emission.

We show that the eMSTO of M11 is visible in the $G_{\rm RP}$ versus $G_{\rm BP}-G_{\rm RP}$ CMD from *Gaia* DR2 photometry. Driven by this finding, we started to search for multiple populations in Galactic open clusters by using this data set and found eMSTOs in NGC 2099, NGC 2360, and NGC 2818.

Our results indicate that the eMSTO is not a peculiarity of the extragalactic MC clusters but is a common feature of Galactic open clusters, thus challenging the traditional idea that these objects are the proxy of a single isochrone. High-resolution spectroscopy has provided direct evidence that stellar rotation is the major factor responsible for the split MS and the eMSTO in open clusters, making these objects similar to MCs clusters.

The authors thank the referee for insightful comments. A.F.M. and L.C. acknowledge support by the Australian Research Council through Discovery Early Career Researcher Award DE160100851 and the Future Fellowship FT160100402. A.P.M. has been supported by the European Research Council through the Starting Grant "GALFOR" (716082) and the FARE-MIUR project R164RM93XW "SEMPLICE". A.S., L.B.N., and F.V. are partially supported by the MINECO (Spanish Ministry of Economy) through grants ESP2017-82674-R and ESP2016-80079-C2-1-R (MINECO/FEDER, UE), SGR-1131 (Generalitat Catalunya), and MDM-2014-0369 of ICCUB (Unidad de Excelencia "María de Maeztu").

ORCID iDs

A. F. Marino https://orcid.org/0000-0002-1276-5487
A. P. Milone https://orcid.org/0000-0001-7506-930X
L. Casagrande https://orcid.org/0000-0003-2688-7511

References

Anderson, J., & King, I. R. 2000, PASP, 112, 1360
Anderson, J., Sarajedini, A., Bedin, L. R., et al. 2008, AJ, 135, 2055
Bastian, N., Cabrera-Ziri, I., Niederhofer, F., et al. 2017, MNRAS, 465, 4795

Bastian, N., & de Mink, S. E. 2009, MNRAS, 398, L11
Bedin, L. R., Salaris, M., King, I. R., et al. 2010, ApJL, 708, L32
Brandt, T. D., & Huang, C. X. 2015a, ApJ, 807, 24
Brandt, T. D., & Huang, C. X. 2015b, ApJ, 807, 58
Butler, K., & Giddings, J. R. 1985, Newsletter of Analysis of Astronomical Spectra, No. 9 (London: Univ. London)
Cantat-Gaudin, T., Jordi, C., Vallenari, A., et al. 2018, arXiv:1805.08726
Cantat-Gaudin, T., Vallenari, A., Zaggia, S., et al. 2014, A&A, 569, A17
Casagrande, L., Silva Aguirre, V., Stello, D., et al. 2014, ApJ, 787, 110
Conroy, C., & Spergel, D. N. 2011, ApJ, 726, 36
Correnti, M., Goudfrooij, P., Bellini, A., Kalirai, J. S., & Puzia, T. H. 2017, MNRAS, 467, 3628
Correnti, M., Goudfrooij, P., Puzia, T. H., & de Mink, S. E. 2015, MNRAS, 450, 3054
D'Antona, F., Di Criscienzo, M., Decressin, T., et al. 2015, MNRAS, 453, 2637
D'Antona, F., Montalbán, J., Kupka, F., & Heiter, U. 2002, ApJL, 564, L93
Dupree, A. K., Dotter, A., Johnson, C. I., et al. 2017, ApJL, 846, L1
Gaia Collaboration, Brown, A. G. A., Vallenari, A., et al. 2018, A&A, 616, A1
Georgy, C., Ekström, S., Eggenberger, P., et al. 2013, A&A, 558, A103
Giddings, J. R. 1981, PhD thesis, Univ. London
Gilmore, G., Randich, S., Asplund, M., et al. 2012, Msngr, 147, 25
Glatt, K., Grebel, E. K., Sabbi, E., et al. 2008, AJ, 136, 1703
Goudfrooij, P., Girardi, L., Kozhurina-Platais, V., et al. 2014, ApJ, 797, 35
Goudfrooij, P., Puzia, T. H., Kozhurina-Platais, V., & Chandar, R. 2011, ApJ, 737, 3
Huang, W., Gies, D. R., & McSwain, M. V. 2010, ApJ, 722, 605
Kalirai, J. S., Fahlman, G. G., Richer, H. B., & Ventura, P. 2003, AJ, 126, 1402
Keller, S. C., Bessell, M. S., & Da Costa, G. S. 2000, AJ, 119, 1748
Keller, S. C., Mackey, A. D., & Da Costa, G. S. 2011, ApJ, 731, 22
Kurucz, R. L. 1993, CD-ROM No. 13 (Cambridge, MA: SAO)
Li, C., de Grijs, R., Deng, L., & Milone, A. P. 2017, ApJ, 844, 119
Mackey, A. D., & Broby Nielsen, P. 2007, MNRAS, 379, 151
Marigo, P., Girardi, L., Bressan, A., et al. 2017, ApJ, 835, 77
Marino, A. F., Przybilla, N., Milone, A. P., et al. 2018, arXiv:1807.04493
Meynet, G., & Maeder, A. 2000, A&A, 361, 101
Milone, A. P., Bedin, L. R., Cassisi, S., et al. 2013, A&A, 555, A143
Milone, A. P., Bedin, L. R., Piotto, G., & Anderson, J. 2009, A&A, 497, 755
Milone, A. P., Marino, A. F., D'Antona, F., et al. 2016, MNRAS, 458, 4368
Milone, A. P., Marino, A. F., Di Criscienzo, M., et al. 2018, MNRAS, 477, 2640
Milone, A. P., Marino, A. F., Piotto, G., et al. 2015, ApJ, 808, 51
Milone, A. P., Piotto, G., Bedin, L. R., et al. 2012, A&A, 540, A16
Pasquini, L., Avila, G., Blecha, A., et al. 2002, Msngr, 110, 1
Przybilla, N., & Butler, K. 2004a, ApJ, 609, 1181
Przybilla, N., & Butler, K. 2004b, ApJL, 610, L61
Schlegel, D. J., Finkbeiner, D. P., & Davis, M. 1998, ApJ, 500, 525
Sung, H., Bessell, M. S., Lee, H.-W., Kang, Y. H., & Lee, S.-W. 1999, MNRAS, 310, 982